Journal of Wind Engineering & Industrial Aerodynamics 230 (2022) 105177

Contents lists available at ScienceDirect

Journal of Wind Engineering & Industrial Aerodynamics

journal homepage: www.elsevier.com/locate/jweia

Influence of position and wind direction on the performance of a roof mounted vertical axis wind turbine

Yannick Jooss, Eivind Berg Rønning, R. Jason Hearst, Tania Bracchi *

Norwegian University of Science and Technology, Department of Energy and Process Engineering, Norway

ARTICLE INFO

Keywords:
Urban wind energy
Wind tunnel measurements

ABSTRACT

The ideal position for a roof mounted wind turbine is investigated experimentally in a wind tunnel. The set-up consists of two cube-shaped buildings. A Savonius (drag driven) vertical axis wind turbine is placed on one of the buildings and its position is varied. Three different locations on the cube and two different turbine heights are examined. Wind from five directions is simulated to obtain a holistic characterization of the problem. The performance of the turbine is evaluated directly through measurements of the converted power. This is complemented by measurements of the surface pressure on the cubes to gain insight into the flow field. A central position on the building was found to maximize the power output for a uniform wind rose, independent of the turbine height. Placing the turbine higher above the roof increased performance for wind normal to the faces of the buildings, while a lower position showed slight advantages for the other wind directions. Overall improved performance for the roof mounted wind turbine was observed compared to the same turbine without a cube present.

1. Introduction

In an effort to mitigate the impact of climate change, nations worldwide agreed on limiting the global temperature increase to 1.5 °C (UNFCCC, 2015). A focal point in this process is the transition to renewable energies (Chang et al., 2017) with wind energy as a key energy source (Porté-Agel et al., 2020). Compared to utility scale implementations of wind energy, little attention has been given to installations in the built environment (Walker, 2011; Toja-Silva et al., 2015). The wind resources in such areas are complex and large installations are difficult to realize. However, there are also advantages to this path, namely a reduction of transmission losses and simplified distribution infrastructure (Kc et al., 2019). One of the key points to address in order to advance this technology further is to develop a better understanding of urban wind resources (Toja-Silva et al., 2015; Stathopoulos et al., 2018; Kc et al., 2019; Rezaeiha et al., 2020; Škvorc and Kozmar, 2021). The two lowest layers in the urban atmosphere are the urban canopy from the ground up to building height and the roughness sublayer above that Oke (1976). The urban canopy is dominated by microscale effects leading to complex flows (Wang et al., 2014) and low mean velocities. Thus, wind turbines in the built environment are typically placed above roof level in the roughness sublayer (Millward-Hopkins et al., 2012), which extends up to 2–5 building heights (h) above the ground (Raupach et al., 1991). This makes roof mounted installations an attractive option (Zhang et al., 2022). No large towers are required and no additional space on the ground is occupied.

Topics of interest for roof mounted wind turbines are the influence of different turbine types (Danao et al., 2013; Scheurich and Brown, 2013; Wekesa et al., 2016; Loganathan et al., 2017; Aliferis et al., 2019), roof shape (Ledo et al., 2011; Abohela et al., 2013; Toja-Silva et al., 2015; Shahizare et al., 2016; Zhou et al., 2017) and position relative to the building (Mertens, 2003, 2006; Ledo et al., 2011; Abohela et al., 2013; Allard and Paraschivoiu, 2022). Mertens (2003) made a first attempt at assessing the potential energy of roof mounted wind turbines for flat roof buildings. The importance of the recirculation bubble growing on top of the roof was stressed. This induces a skew angle in the mean flow, which varies along the roof, and a region of accelerated flow on top of the recirculation bubble. A central location was found to be ideal to maximize the energy density while minimizing the skew angle for a uniform wind rose. In a related work, Mertens (2006) showed that an increased skew angle can be beneficial for lift-driven vertical axis wind turbines (VAWTs). This led to the conclusion that for lift-driven VAWTs the windward edge would be the ideal position. Ledo et al. (2011) examined an array of buildings and found that flat roofs lead to both higher velocities and lower turbulence intensities above the buildings compared to pitched and pyramidal roof shapes. Thus, they recommended installation on

* Corresponding author.
E-mail addresses: yannick.jooss@ntnu.no (Y. Jooss), tania.bracchi@ntnu.no (T. Bracchi).

https://doi.org/10.1016/j.jweia.2022.105177
Received 11 April 2022; Received in revised form 29 August 2022; Accepted 14 September 2022

a flat roof, where all investigated positions (edge, corner and centre) were concluded to be suitable locations, whereas on pyramidal roofs only the edge was deemed suitable. On a pitched roof no location was deemed suitable. Abohela et al. (2013) analysed flat, spherical, gabled, pyramidal, vaulted and pitched roofs. A region of accelerated flow was found for all shapes. This lead to a maximal increase in available power between 26% for pyramidal and 56.1% for vaulted roofs. A standard flat roof building yielded up to 40.5% increase in available wind power. When finding the optimal position, turbine heights below 30% of the building height above the roof were ignored, due to the increased turbulence in this region. This lead to ideal heights 30%–60% h above the roof. Toja-Silva et al. (2015) looked at flat, spherical, vaulted and pitched roof shapes. The roof edge geometry was also varied for the flat roofs. Sharp and curved edges as well as vertical and horizontal overlapping railings were examined. Curved shapes were found to be beneficial for the available energy for both the roof shape and the edges while a vertical railing was shown to enlarge the recirculation area. Allard and Paraschivoiu (2022) investigated the power output of Darrieus-type (lift-driven) VAWTs on a cubic building. For wind facing the corner of a cube an increase in power coefficient compared to undisturbed flow was found, particularly for a position on one of the adjacent corners.

The aforementioned studies relied primarily on RANS simulations, thus there is a need for experimental studies (Kc et al., 2019). Al-Quraan et al. (2016) and Škvorc and Kozmar (2021) recommend wind tunnel measurements as a potential tool that can provide a good approximation of real urban wind energy problems. Šarkić Glumac et al. (2018) investigated the wind energy potential above a high rise building with hot-wire measurements in a wind tunnel. The influence of four surrounding buildings with a distance of two building widths was also examined. Wind facing the corner was found to be favourable for the available wind power. In a subsequent study on the same set-up, Vita et al. (2020) found that wind turbine heights larger than 0.3 building widths above roof height were preferable, where accelerated flow was measured and the recirculating flow close to the roof was avoided. However, it was also identified that this involves significant complications to the installations as the wind turbines need to be placed on tall masts mounted to the building roofs. Thus, investigating turbine heights lower than that carries significance. Zhang et al. (2022) investigated a cluster of horizontal axis wind turbines on an array of cubes in a large eddy simulation. Actuator disks were used to model the turbines. The turbine diameter was $d_T = 0.25h$, and three hub heights between $0.375h$ and $0.875h$ above the roof were considered. This extends the rotor swept area down to $0.125h$ above the roof. A significant area of acceleration was detected above the cube array. A turbine height of $0.625h$ above the roof was found to be ideal, but the power output was within 10% for all three heights.

The upstream blockage a wind turbine generates has a measurable impact on the available power (Medici et al., 2011; Yan et al., 2018; Porté-Agel et al., 2020). In a recent study (Jooss et al., 2022), showed that for roof mounted wind turbines the influence of the wind turbine itself is especially significant and hard to predict. Most of the aforementioned studies investigating the ideal roof position do not take into account the presence of a turbine itself, instead they solely rely on velocity measurements. The use of actuator disks can partially compensate for this (Ge et al., 2021; Zhang et al., 2022). However, the full complexity of a rotating energy extracting machine remains hard to replicate. Thus, in the present study a small vertical axis wind turbine is placed on a model building. Furthermore, the influence of an identical neighbouring building $2h$ away is examined. Based on power measurements the ideal location for a roof mounted wind turbine is then evaluated. VAWTs have received increasing attention overall (Dabiri, 2011; Shamsoddin and Porté-Agel, 2014) and are considered to be well suited for the urban environment (Kooiman and Tullis, 2010; Li et al., 2010; Hui et al., 2018). VAWTs for buildings are commercially available from, for example, Aeolos, CleanVerTec, Quietrevolution, Greener Energy, Semtive and the Solar Impulse Foundation. In fact, they have become so common that they can be directly purchased by consumers on Amazon. Typical wind turbine heights (h_T) are between 1 m and 6 m, resulting in size ratios on one storey and three storey buildings of $0.23 \lesssim h_T/h \lesssim 1.44$ and $0.08 \lesssim h_T/h \lesssim 0.62$, respectively.

Surface mounted cubes are used to model the buildings in the present study. This is a common approach to model residential buildings both in simulations and wind tunnel studies (Millward-Hopkins et al., 2012; Abohela et al., 2013; Ge et al., 2021; Zhang et al., 2022; Allard and Paraschivoiu, 2022; Jooss et al., 2022). However, the range of applications for flow around cubes is wide, thus making it an extensively studied topic. This ranges from single cubes (Castro and Robins, 1977; Yakhot et al., 2006; Hearst et al., 2016; Kozmar, 2020, 2021) to cube arrays (Meinders and Hanjalić, 1999; Cheng et al., 2003; Xie and Castro, 2006; Xie et al., 2008; Ferreira and Ganapathisubramani, 2021). Particularly relevant to the present work are the studies by Castro and Robins (1977), Martinuzzi and Havel (2004), Gao et al. (2021) and Jooss et al. (2022). Castro and Robins (1977)'s study of a single surface mounted cube subjected to various inflow velocity profiles and wind directions is used to illustrate the fundamental difference between the flow around a cube for inflow from $\theta = 0°$, normal to a face of the cube, compared to $\theta = 45°$. Martinuzzi and Havel (2004) and Jooss et al. (2022) examined the flow around two cubes in tandem formation with a cube spacing of $s/h = 2$ and thus provide information on the flow field for $\theta = 0°$ and 180°. While (Martinuzzi and Havel, 2004) give a holistic image of the flow field, Jooss et al. (2022) provide a detailed analysis along the centre plane of the cubes using particle image velocimetry (PIV).

A set-up with two buildings represented by cubes spaced $s/h = 2$ was used in the present work. The performance of a Savonius (drag-driven) VAWT was examined at three different locations and five different wind directions. In addition, two different turbine heights were used, yielding a total of 30 experimental cases. From this it was possible to identify favourable wind directions and assess the ideal position both for individual wind directions and holistically.

2. Experimental procedure

The experimental set-up consists of two $h = 100$ mm cubes representing idealized buildings with a small VAWT of the Savonius (drag) type on top. The set-up is based on a previous study by Jooss et al. (2022). The cubes were placed in line with each other separated by $2h$ on a circular flat plate, which was used as an artificial floor. A schematic of this is shown in Fig. 1 (a). The plate has a diameter of 1.4 m and a thickness of 10 mm. It was placed in the large scale wind tunnel at the Norwegian University of Science and Technology. This is a closed loop recirculating tunnel with a test section of 2.71 m × 1.80 m × 11.15 m (width × height × length). The plate was mounted on legs and elevated from the wind tunnel floor to lift it above the naturally occurring floor boundary layer. The edge of the plate was sharpened to a 15° angle on the bottom to minimize flow separation. A 2 mm wire placed 100 mm from the edge was used to trip the boundary layer to create a repeatable and constant transition point. The flow velocity in the tunnel was kept constant at $U_\infty = 9.05$ m/s ±0.05 m/s corresponding to a Reynolds number $Re_h = U_\infty h/\nu$ of approximately 60 000. U_∞ was measured with a Pitot-static tube and the viscosity, ν, was calculated based on the air temperature. The changes in temperature and atmospheric pressure were tracked with a K-type thermocouple and a mercury barometer. To simulate varying wind directions, θ, the plate was rotated from $\theta = 0°$ to $\theta = 180°$ in 45° steps, where $\theta = 0°$ refers to the case with the turbine on the upstream cube, and $\theta = 180°$ to the one with the turbine on the downstream cube. Three different wind turbine positions on the cube were examined and are hereafter referred to as position 1, 2 and 3, as illustrated in Fig. 1(a). The coordinate system is fixed on the plate in the centre of the examined cube. In addition, the distance between the turbine blades and the roof of the cube was varied from a low (L)

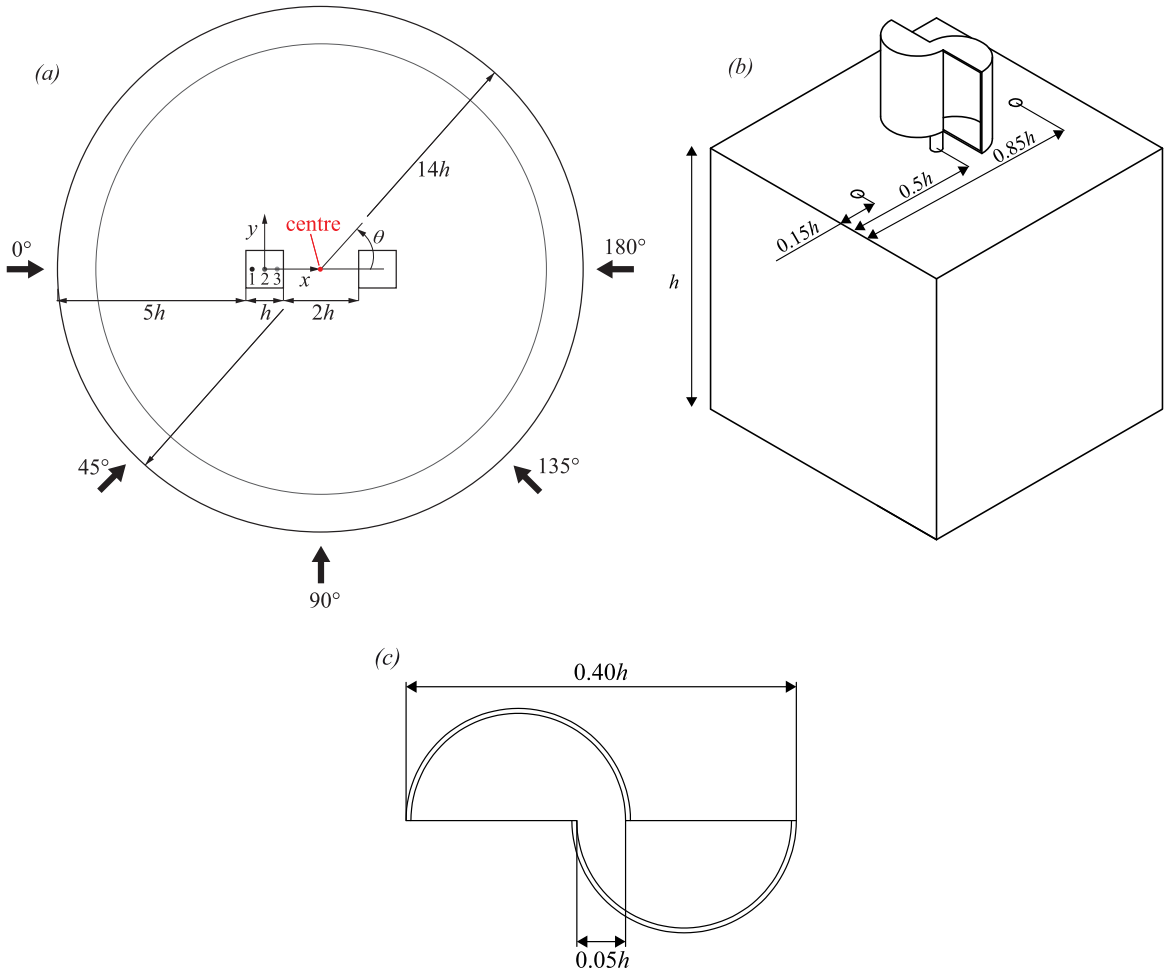

Fig. 1. Geometrical set-up: (*a*) displays the positions of the cubes on the plate and the examined wind directions, (*b*) shows the low turbine on the cube and its relative positions (Jooss et al., 2022), (*c*) gives the cross section of the Savonius type vertical axis wind turbine (Jooss et al., 2022).

position at $0.08h$ to a high (H) position at $0.16h$, which gives turbine centre heights of $0.23h$ and $0.31h$ above the roof, respectively. The combination of incoming wind angles, turbine placement positions, and turbine mounting heights yields a total of 30 examined cases.

Larin et al. (2016) show that, with the right configuration, Savonius (drag) type turbines can be a promising option for roof-mounted wind turbines. In the present study a generic two bucket Savonius turbine inspired by Alexander and Holownia (1978) and Akwa et al. (2012) was used. Note, that it is not the objective of this study to optimize the turbine design. It is made out of polylactide (PLA). The design is shown in Fig. 1 (*b*) and 1 (*c*) and is identical to the design used in Jooss et al. (2022). The turbine has a diameter d_T of $0.4h$ and a blade height of $0.3h$. This yields a size ratio to the building which is representative for VAWT installations on one to three storey buildings (see Section 1). Its blades consist of two overlapping semi-circles. The overlap helps to decrease the starting torque (Kumbernuss et al., 2012). The resulting wind turbine's Reynolds number $Re_{d_T} = U_\infty d_T/\nu$ based on the turbine diameter is 24000.

To evaluate the performance of the turbine and to control its operation, a brushed DC motor (12G88 Athlonix) was used as a generator. The circuit is shown schematically together with a picture of the set-up in Fig. 2. The generated current, I, was measured over a 0.1 Ohm shunt resistor with an INA219 High Side DC Current Sensor. I is directly proportional to the electromagnetic torque, $Q_e = K_T I$, where K_T is the torque constant of the motor. The rotational velocity, Ω, of the turbine was measured with a reflective object sensor (OPB705WZ). An infrared emitter and a phototransistor were used to detect the partly reflective shaft of the turbine. Thus, the converted power, $P_c = Q_e\Omega$, can be calculated. This is a good measure of the mechanical power, $P_m = P_c + P_f$, which is only different from P_c by the friction losses, P_f, which can be estimated based on the motor data (Bastankhah and Porté-Agel, 2017). Drag driven VAWTs are generally run at relatively low tip-speed-ratios, $\lambda = \frac{\Omega r_T}{U}$, which is the velocity of the blade tip relative to the flow velocity. This is where friction losses become less relevant (Bastankhah and Porté-Agel, 2017). A high frequency variable switch (IRF540NPbF) operated through an Arduino Uno was used to control the turbine. By opening and closing the switch at a set frequency, the rotational velocity of the turbine was controlled. A similar method was employed in recent studies by Gambuzza and Ganapathisubramani (2021) and Jooss et al. (2022). Full power curves with a minimum of 10 operating points per curve were acquired for every case. An uncertainty analysis including both systematic and random errors based on (Wheeler and Ganji, 1996) was carried out.

To obtain information on the flow around the cubes for the different wind directions, the surface pressure was measured with 61 pressure taps distributed on the examined cube. The pressure was measured with a Scanivalve MPS4264 miniature pressure scanner. The static port of a Pitot-static tube was used as a reference. All ports were sampled simultaneously for 60 s at a frequency of 800 Hz.

3. Flow field

The focus of this study is on the performance of the wind turbine at different positions on the cube for varying wind directions. In a

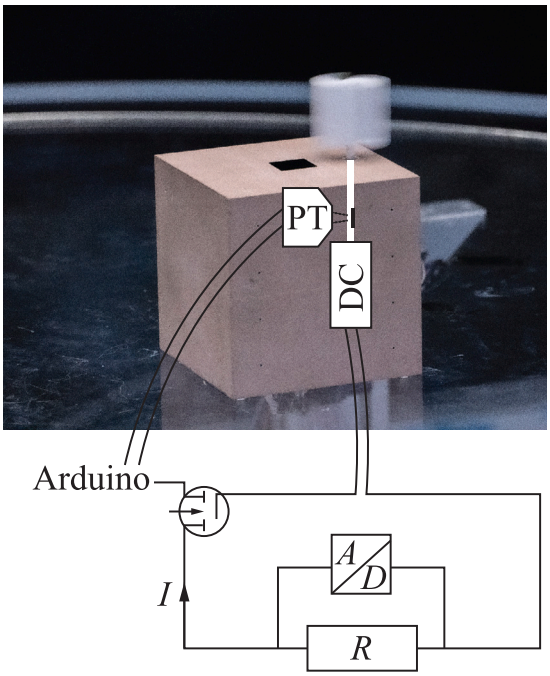

Fig. 2. Schematic of the experimental set-up to measure the converted power P_c of the wind turbine and control its tip speed ratio.

preceding study using a similar set-up it was shown that the turbine performance should be measured directly and cannot easily be deduced from velocity measurements at the turbine position (Jooss et al., 2022). Basing power estimates on the flow field without a turbine present led to significant discrepancies. Thus, to evaluate the ideal position of a roof mounted VAWT, the actual power output of a turbine should be measured. Nevertheless, it is useful to have a fundamental understanding of the flow patterns that occur in this set-up to explain the results and draw conclusions on the general applicability.

The flow on top of the plate was first examined without the cubes and turbine present. For this a velocity profile at $x/h = -0.5$, the position of the windward edge of the upstream cube for $\theta = 0°$, and $y/h = 0$ was obtained with a Pitot-static boundary layer probe. See Fig. 1 for the coordinate system. Fig. 3 (*a*) shows the resulting velocity profile. The boundary layer thickness, δ, where the velocity is 99% of the freestream velocity is $\delta/h = 0.32$. Above that the velocity profile is uniform. This is by design to have generic and reproducible inflow conditions. The turbulence intensity in the freestream was measured with a Dantec 55P21 X-wire probe and found to be $u'_\infty/U_\infty = 1.1\%$, where u'_∞ is the standard deviation of the turbulent fluctuations in the freestream. The integral length scale normalized by the building height is $L_{u,\infty}/h = 0.49$ and the Reynolds shear stress is effectively zero at $\frac{\overline{u'_\infty w'_\infty}}{U_\infty^2} = 1.2 \times 10^{-5}$. The energy spectrum of the streamwise velocity in the freestream, normalized by the Kolmogorov length scale (η) and the viscosity (ν) is shown in Fig. 3 (*b*). Although we provide the turbulence statistics for reference, the flow is intended to be a low-turbulence, quasi-laminar flow that is easily reproducible in other facilities and in computational fluid dynamics simulations.

The surface pressure is measured on the cube to obtain a qualitative understanding of the flow regions arising for the different wind directions. Fig. 4 (*a*) shows a comparison of the pressure coefficient $C_p = \frac{p_s - p_\infty}{\frac{1}{2}\rho U_\infty}$ along the centre line of the upstream cube for $\theta = 0°$ with data from a single cube by Castro and Robins (1977), where p_s, p_∞ and ρ are the surface static pressure, the freestream static pressure and the air density, respectively. Castro and Robins (1977) examined two different inflow velocity profiles, one with a uniform velocity field upstream of the cube, similar to the present study, and one where the cube was immersed in the boundary layer. The measurements by Castro and Robins (1977) have finer spatial resolution, nonetheless it is apparent that the present measurements follow the C_p of the uniform inflow well. There are slight deviations in the lower part of the windward face ($0 \leqslant l/h \leqslant 1$), where the present study records lower C_p compared to the reference data with uniform inflow. C_p is closer to the boundary layer case here, which presumably originates from a slightly larger δ in the present study compared to the uniform case by Castro and Robins (1977). On the roof ($1 \leqslant l/h \leqslant 2$), which is the most relevant area for this study, the measurements collapse with the uniform inflow case by Castro and Robins (1977). This indicates a similar flow on top of the upstream cube compared to a single cube and suggests limited influence of the boundary layer as long as it is thin. On the leeward face the agreement is still strong with slightly higher C_p-values in the present study, which is expected due to the presence of the second cube.

Jooss et al. (2022) conducted high-fidelity velocity measurements on a similar set-up using PIV for $\theta = 0°$. This information can be complemented with hot-wire measurements above the centre of the cube ($x/h = 0$, $y/h = 0$) for $\theta = 0°$ and $\theta = 45°$ by Castro and Robins (1977). These measurements are plotted together with the swept area of the two examined turbine heights in Fig. 4 (*b*). A good agreement between (Jooss et al., 2022) and Castro and Robins (1977) for $\theta = 0°$ can be observed, which again underlines the similarity between the flow above the upstream cube and the flow above a single cube. The comparison between the velocity profiles for $\theta = 0°$ and $\theta = 45°$ shows significant differences in the region where the turbines are placed. The full flow field along the centre plane from Jooss et al. (2022) is shown in Fig. 5. For $\theta = 0°$ the flow separates at the windward top edge of the cube and a large area of recirculating flow emerges on top of the cube. This results in low velocities and partly reverse flow up to $z/h \approx 1.4$. For $\theta = 45°$ the measurements by Castro and Robins (1977) at the centre of the cube do not indicate any flow separation, with the velocities exceeding the freestream velocities throughout the entire swept area for both turbine heights. The velocity surplus is higher closer to the roof and approaches U_∞ with increasing distance.

Fig. 6 shows C_p on the roof of the cube for the different wind directions. These measurements were conducted without the turbine present. The locations of the pressure taps are marked with circles, black at the turbine locations, white for the additional taps. From this a contour map is approximated through linear interpolation between the pressure taps. This is done only to obtain a qualitative illustration of the flow patterns on top of the roof. A detailed analysis would require a finer discretization. However, general trends can still be identified from this. The flow field for $\theta = 0°$ and $\theta = 180°$ has been described in Jooss et al. (2022), as shown in Fig. 5. Upstream of the first cube the flow decelerates and at the bottom edge a horseshoe vortex forms (Castro and Robins, 1977; Martinuzzi and Havel, 2004; Kozmar, 2021). At the top leading edge the flow separates and a large region of recirculating flow arises on top of the first cube and downstream of it. This manifests in low and relatively constant values of C_p in Fig. 6 (*a*). Similar observations were made for the roof of a single high rise building by Šarkić Glumac et al. (2018). For wind from $\theta = 180°$ the examined cube is in the wake of an upstream cube (Jooss et al., 2022). The flow intermittently reattaches on top of the examined cube, leading to higher but still relatively constant C_p. Flow from $\theta = 45°$ on a single cube was examined by, e.g., Castro and Robins (1977), Natarajan and Chyu (1994) and Kozmar (2020) and for a high rise building by Šarkić Glumac et al. (2018). They all report two conical vortices forming along the two top windward edges. This is visible in Fig. 6 (*b*) with very low C_p where the flow separates. These studies also show that the flow along the diagonal of the cube in the direction of the flow does not fully separate. This is apparent looking at the velocity profile by Castro and Robins (1977) for $\theta = 45°$ in Fig. 4 (*b*). The slight asymmetry presumably comes from the influence of the downstream cube. This asymmetry is even

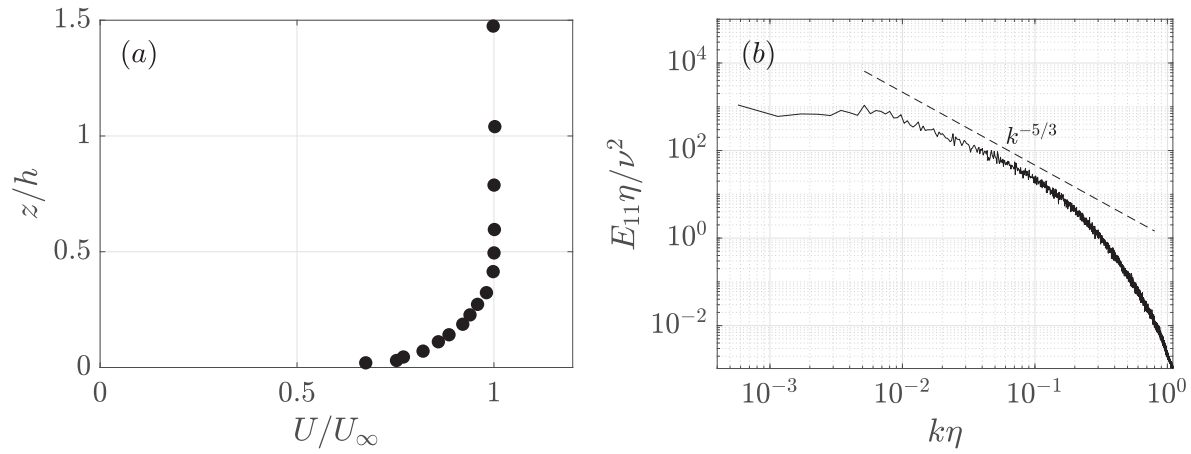

Fig. 3. (*a*) Incoming velocity profile measured at the windward edge of the first cube $x/h = -0.5$. (*b*) Spectral distribution of energy of the streamwise velocity measured in the freestream.

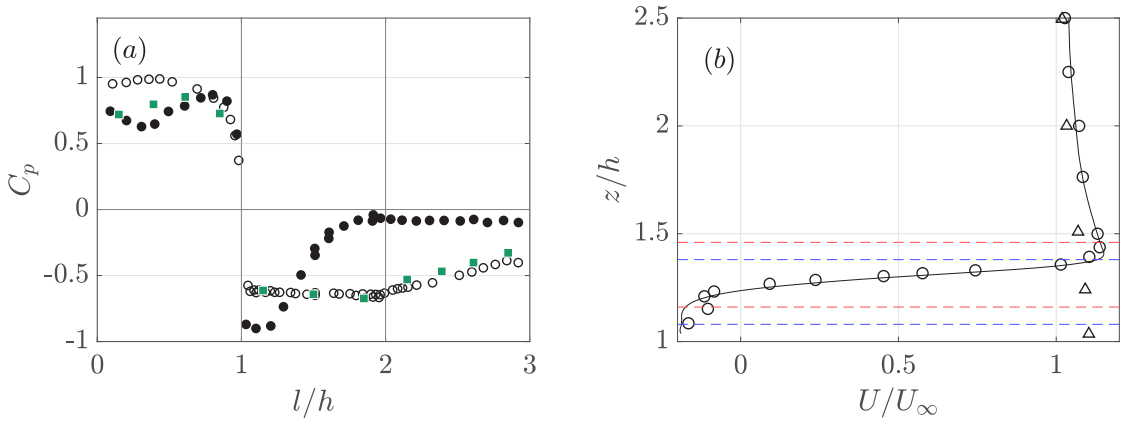

Fig. 4. (*a*) Comparison of surface pressure measurements along the centre-line of the set-up with reference data from a single cube: ∘ (Castro and Robins, 1977) uniform inflow, • (Castro and Robins, 1977) cube immersed in turbulent boundary layer, ■ measurements on the upstream cube of the present set-up for $\theta = 0°$. (*b*) Velocity profiles above the centre of a single cube with uniform inflow: ∘ 0° inflow and △ 45° inflow by Castro and Robins (1977) and — measurements on the upstream cube of the present set-up for 0° inflow measured in a previous study by Jooss et al. (2022). The turbine's swept area is marked with - - for the low turbine and - - for the high turbine. *l* follows the centre line of the cube, starting from the windward bottom edge to the top, along the roof and down to the leeward bottom edge.

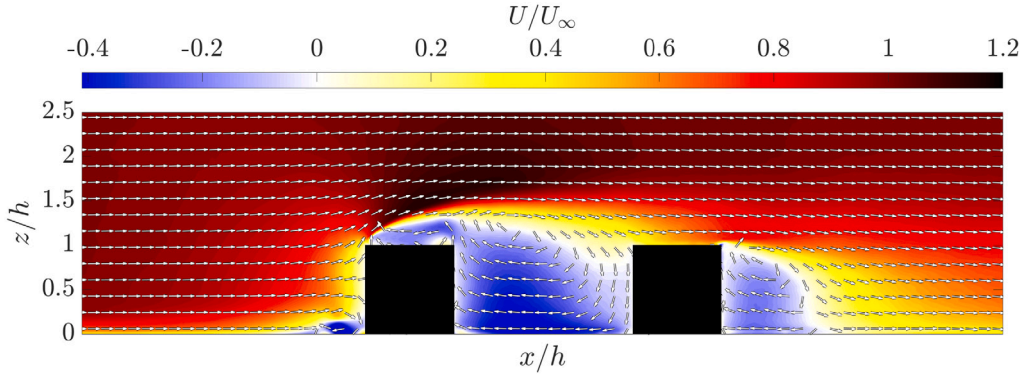

Fig. 5. Flow field of streamwise velocity U from Jooss et al. (2022) for $\theta = 0°$ (and 180°).

more pronounced for $\theta = 135°$, where the neighbouring cube now is upstream of the examined cube. In principle, the same structure as for $\theta = 45°$ is visible. For $\theta = 90°$, again the flow separates on the top windward edge. However, here also an asymmetry from left to right is observed. This is due to the neighbouring cube located on the right side which causes a deflection and acceleration of the flow towards the examined cube. A more detailed analysis on this flow case was conducted in a recent study by Gao et al. (2021) investigating the flow around a pair of neighbouring cubes. The acceleration of the streamwise velocity on the inside of the cube compared to the outside

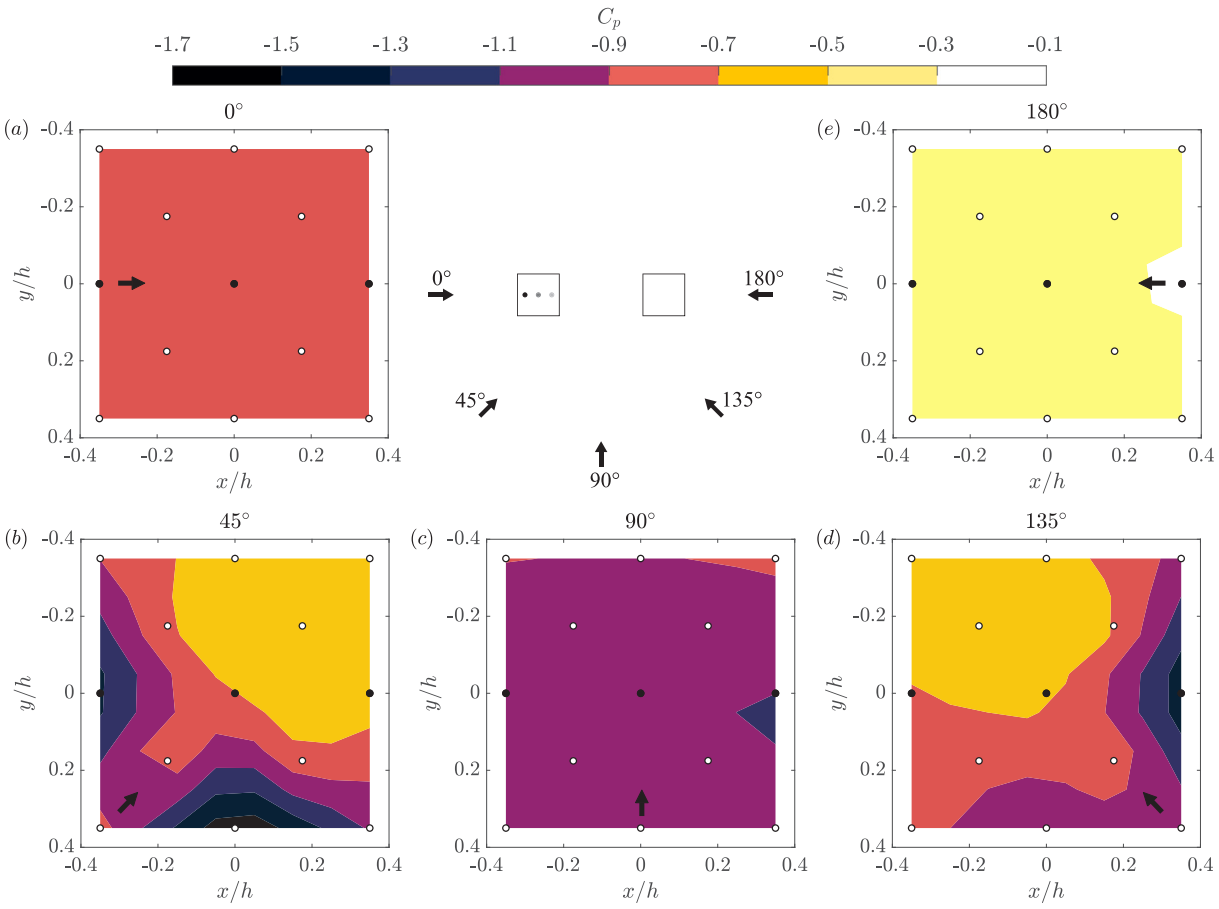

Fig. 6. Mean surface pressure coefficient C_p on the roof of the investigated building for different wind directions without the turbine present. The locations of the pressure taps are marked with circles, black at the turbine locations, white for the additional taps. The contour maps are linearly interpolated from these measurements.

for spacings $1 < s/h < 2.5$ was shown and they explicitly demonstrated that this also leads to accelerated flow on top of the cube close to the edge facing the neighbouring cube.

4. Power measurements

4.1. Reference freestream measurements

As a reference the power output of the turbine in undisturbed flow without the cubes was measured. The power coefficient, $C_P = \frac{P_m}{\frac{1}{2}\rho U_\infty^3 A}$, is presented in Fig. 7. The reference case is denoted with $_0$. The maximum errors for C_P and λ were found to be 3.5% and 1.5%, respectively. In the following, all power curves are given with error bars. At $\lambda = 0.35$ the maximum power output is observed with $C_{P0,max} = 0.042$. The power curve spans from $\lambda \approx 0.1$ to $\lambda \approx 0.7$. The shape of the power curve resembles those found in literature (Alexander and Holownia, 1978; Akwa et al., 2012; Aliferis et al., 2019). Savonius type turbines have generally low power coefficients, up to $C_P = 0.3$, and the power output scales strongly with Reynolds number (Akwa et al., 2012; Aliferis et al., 2019). This explains the low observed C_P-values for this miniature turbine.

To enable an assessment of the roof mounted turbine at different locations, C_P is always calculated based on U_∞. Figs. 8 and 9 show the C_P-curves for the low (L) and high (H) turbine at three different positions (1, 2 and 3), for the five different wind directions ($0° \leq \theta \leq 180°$). This gives the cases L1, L2, L3, H1, H2 and H3 for every wind direction. $C_{P\,max}$ is used to compare the different cases to each other.

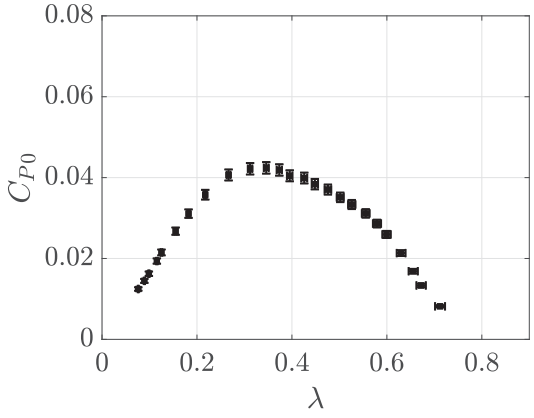

Fig. 7. Reference power curve in a configuration without the cubes present.

4.2. Low turbine

For wind from $\theta = 0°$, L1 gives the maximum C_P of 0.036, with a 23% reduction to L2 at the centre of the cube and a 85% reduction to L3 at the back. This is a significant spread caused by the change of the turbine's position relative to the large area of separated, recirculating flow on top of the first cube. At position 1 the flow is still relatively unaffected by the presence of the cube, indicated by a C_P only slightly below the reference case, whereas farther downstream at L2 and L3 the turbine moves continuously deeper into the growing area of recirculating flow.

Wind from $\theta = 45°$ leads to higher C_P up to 0.06 at L2, and a reduced spread between the three positions of 13%. The power curves for L1 and L2 collapse quite well. At L3 the turbine yields slightly lower power output. The improved performance compared to $\theta = 0°$ can be explained by the absence of a pronounced area of separated flow. This is apparent when looking at the velocity profiles on top of a single cube at its centre for $\theta = 0°$ and $\theta = 45°$ measured by Castro and Robins (1977) in Fig. 4 (*b*). The difference in experienced velocity especially for the low turbine is significant.

A similar flow case occurs for $\theta = 135°$. L1 and L3 are flipped by virtue of rotation, position 1 is now farther downstream on the cube experiencing more separated flow and thus records lower C_P. Generally, the C_P is slightly lower for $\theta = 135°$ than for $\theta = 45°$ which can be explained by the presence of the second cube which creates a region of reduced velocities in its wake. The turbines are now partly placed in this region. This also explains the slightly reduced power output for L3 compared to position L2. Position 3 is located closer to the upstream cube and is thus more affected by its wake.

Wind from $\theta = 90°$ presents a similar case as $\theta = 0°$, but instead of a second cube downstream there is one next to the examined cube. For L2 at the centre of the cube, the turbine yields a $C_{P_{max}}$ of 0.041 which is more than 30% higher than for $\theta = 0°$. While the upstream blockage effect of the downstream cube certainly contributes to this discrepancy, the larger impact comes from the neighbouring cube at $\theta = 90°$. This is evident when considering L1 and L3 as well. While L1 essentially collapses with L2, L3, closest to the neighbouring cube, gives the highest C_P at 0.057, 32% higher than the other two and also significantly higher than any C_P for $\theta = 0°$. This indicates that the neighbouring cube leads to a deflection and acceleration of the flow that is most impactful closest to it. The asymmetry from inside (in between the cubes) to outside is also visible in the surface pressure in Fig. 6 (*c*). This is supported by measurements by Gao et al. (2021), which show the local acceleration of the flow both in between the cubes as well as directly above the roof on the side facing the neighbouring cube.

Flow from $\theta = 180°$ presents, on first glance, a case similar to $\theta = 0°$ and $\theta = 90°$. However, it is fundamentally different, as the cube is positioned firmly in the wake of the upstream cube (see Fig. 5). Thus, the dynamics are governed by a wake flow rather than separating flow. Due to this, L3, the most upstream position in this configuration, has the lowest power output. As the wake recovers further, C_P increases continuously. $\theta = 180°$ is by far the least favourable wind direction for the low turbine with maximal C_P-values between 0.012 and 0.020.

4.3. High turbine

Similar to the low turbine, $\theta = 180°$ is the worst wind direction for the high turbine and it is notable that the C_P-curves do not differ significantly compared to the low turbine with maximum values between 0.016 and 0.021. The spread is reduced between the positions but overall the power output is low for $\theta = 180°$ and the benefit of the high turbine is small.

This is different for wind from $\theta = 0°$. At position 1 there is a moderate C_P increase of 18% for the high turbine compared to the low turbine, with a $C_{P_{max}}$ of 0.044. This increase is more drastic for positions 2 and 3 with 43% and 82%, respectively. This also changes the ideal position for this wind direction. While for the low turbine position 1 at the front of the cube was ideal, for the high turbine it is preferable to place the turbine in position 2 at the centre of the cube. The spread between all three positions is also reduced to 39%. The reason for this is the reduced impact of the recirculation region on top of the cube. The higher turbine experiences more of the high momentum flow on top of the separated flow (see Fig. 4 (*b*)), which leads to higher power output overall and reduced dependency on the position of the turbine on the roof.

Table 1
List of wind turbine performance parameters with comparison to unobstructed reference measurements.

		low			high		
θ	Position	$C_{P_{max}}$	λ_{opt}	$\frac{C_{P_{max}} - C_{P0,max}}{C_{P0,max}}$	$C_{P_{max}}$	λ_{opt}	$\frac{C_{P_{max}} - C_{P0,max}}{C_{P0,max}}$
0°	1	0.036	0.35	-13.9%	0.044	0.33	+5.8%
	2	0.028	0.27	-33.3%	0.049	0.46	+15.9%
	3	0.005	0.16	-87.5%	0.030	0.36	-29.6%
45°	1	0.059	0.37	+40.8%	0.048	0.42	+15.0%
	2	0.060	0.40	+43.0%	0.053	0.37	+26.7%
	3	0.052	0.38	+24.6%	0.049	0.43	+17.1%
90°	1	0.039	0.29	-7.3%	0.050	0.40	+19.4%
	2	0.041	0.35	-2.8%	0.061	0.47	+44.2%
	3	0.057	0.41	+35.6%	0.063	0.47	+49.3%
135°	1	0.044	0.40	+6.1%	0.048	0.39	+13.2%
	2	0.059	0.47	+41.1%	0.056	0.43	+32.8%
	3	0.055	0.37	+30.7%	0.056	0.43	+34.1%
180°	1	0.020	0.29	-52.9%	0.021	0.29	-50.7%
	2	0.017	0.30	-60.7%	0.019	0.31	-54.4%
	3	0.012	0.28	-70.4%	0.016	0.25	-62.8%

For $\theta = 45°$, the spread between the three positions is reduced to 9%. H1 and H3 collapse while H2 yields the highest C_P of 0.053. This is 11% lower than $C_{P_{max}}$ for L2 at $\theta = 45°$. Fig. 4 (*b*) shows that while the velocity immediately above the centre of the roof exceeds the freestream velocity, it approaches U_∞ with increasing distance from the roof. The lower turbine experiences more accelerated flow, which explains the superior performance here.

At $\theta = 135°$ similar trends as for the low turbine are observed. H1, now most downstream on the cube leads to the lowest C_P, whereas H2 and H3 collapse with a $C_{P_{max}}$ of 0.056. This is slightly higher than for $\theta = 45°$. Presumably the high turbine is not as affected by the wake of the other cube and experiences some accelerated flow.

The highest overall performance was measured for the high turbine at $\theta = 90°$ with $C_P = 0.063$ at position 3. H2 produces slightly lower values but essentially collapses with H3. For H1 the maximal C_P is 20% lower. The reason for the superiority of position 3 for $\theta = 90°$ was outlined above for the low turbine. The same applies here; the two cubes side-by-side lead to an acceleration of the flow in-between them, thus benefiting the position closest to the neighbouring cube. Compared to the low turbine, position 2 here collapses not with the inferior position 1 on the outside but essentially with the ideal position 3. This suggests that the region of accelerated flow spreads with increasing distance from the roof, which is supported by an overall reduced spread of 20% for the high turbine compared to 32% for the low turbine at $\theta = 90°$.

4.4. Evaluation

Table 1 lists all results and compares them to the reference measurement $C_{P0,max} = 0.042$ in the unobstructed flow. It is apparent that the lower roof mounted wind turbine performs worse for $\theta = 0°$ and 180°. Favourable wind directions are $\theta = 45°$ and 135° where the performance exceeds $C_{P0,max}$ at every position. This is in agreement with results by Allard and Paraschivoiu (2022). For the high turbine the gain at $\theta = 45°$ and 135° are less significant but $\theta = 90°$ leads to drastic improvements up to 49.3% compared to the reference. $\theta = 0°$ yields comparable $C_{P_{max}}$ to $C_{P0,max}$ for the high turbine and significantly higher values than the low turbine. For $\theta = 180°$, the high turbine performs poorly with reduced $C_{P_{max}}$ compared to the unobstructed reference.

In Table 2 reduced results are presented by assessing the three positions and two turbine heights for all wind directions combined. This is relevant for a uniform or unknown wind rose. Two different

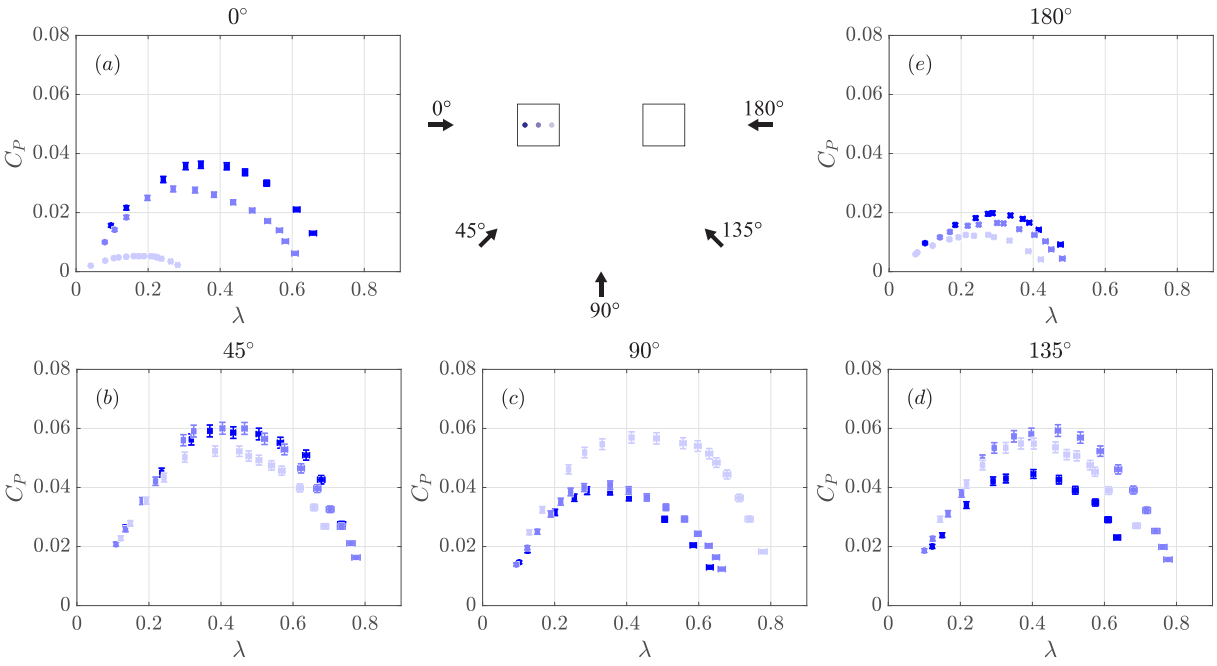

Fig. 8. C_P-curves of the low turbine for different wind directions and positions. L1, L2, L3.

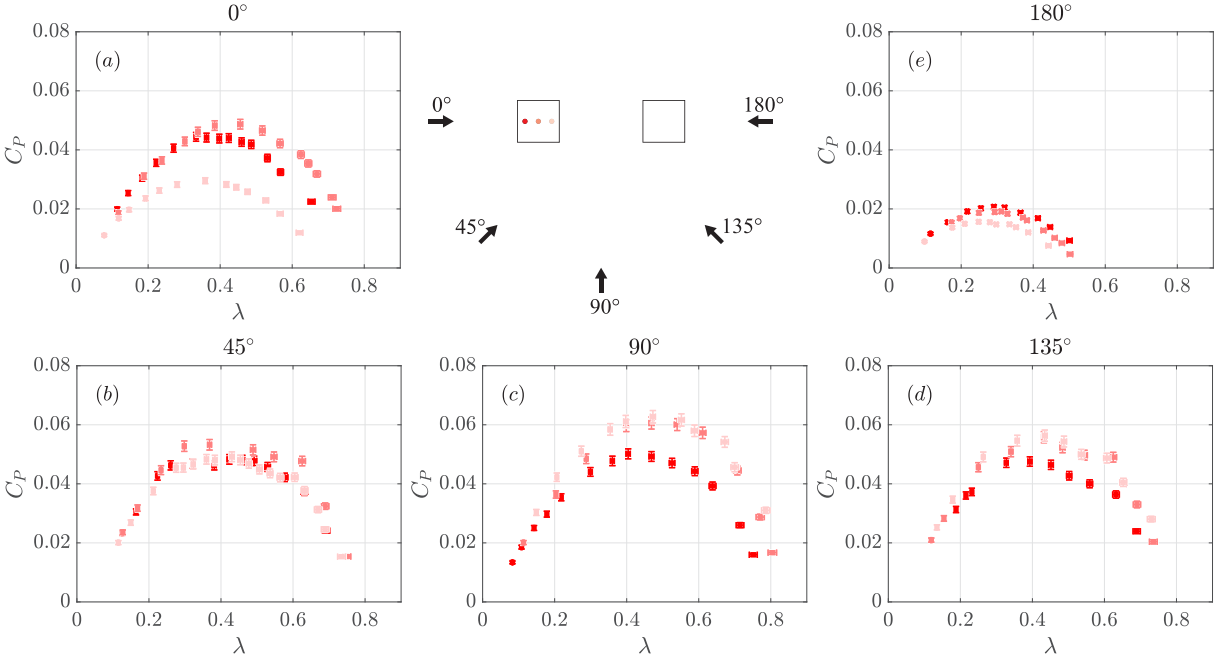

Fig. 9. C_P-curves of the high turbine for different wind directions and positions. H1, H2, H3.

Table 2
Averaged power coefficients for uniform wind rose.

Position	Height	$\langle C_{P\,max} \rangle_\theta$	$\langle \langle C_{P\,max} \rangle_\theta \rangle$	$\int_{0.5\lambda_{opt}}^{1.5\lambda_{opt}} C_P \mathrm{d}\lambda$	$\left\langle \int_{0.5\lambda_{opt}}^{1.5\lambda_{opt}} C_P \mathrm{d}\lambda \right\rangle$	θ_{opt}	Colour
1	low	0.043	0.044	0.014	0.015	45°	
	high	0.045		0.016		90°	
2	low	0.046	0.048	0.016	0.018	45°	
	high	0.051		0.019		90°	
3	low	0.043	0.046	0.015	0.017	90°	
	high	0.048		0.019		90°	

methods of evaluation are presented. The most direct approach is to simply average $C_{P\,max}$ over all wind directions, θ, for a certain position $\langle C_{P\,max} \rangle_\theta$.

To not only take into account peak performance, a method considering a bigger part of the power curve is also included. For this methodology, the C_P-curve was integrated from $0.5\lambda_{opt}$ to $1.5\lambda_{opt}$. Changing the

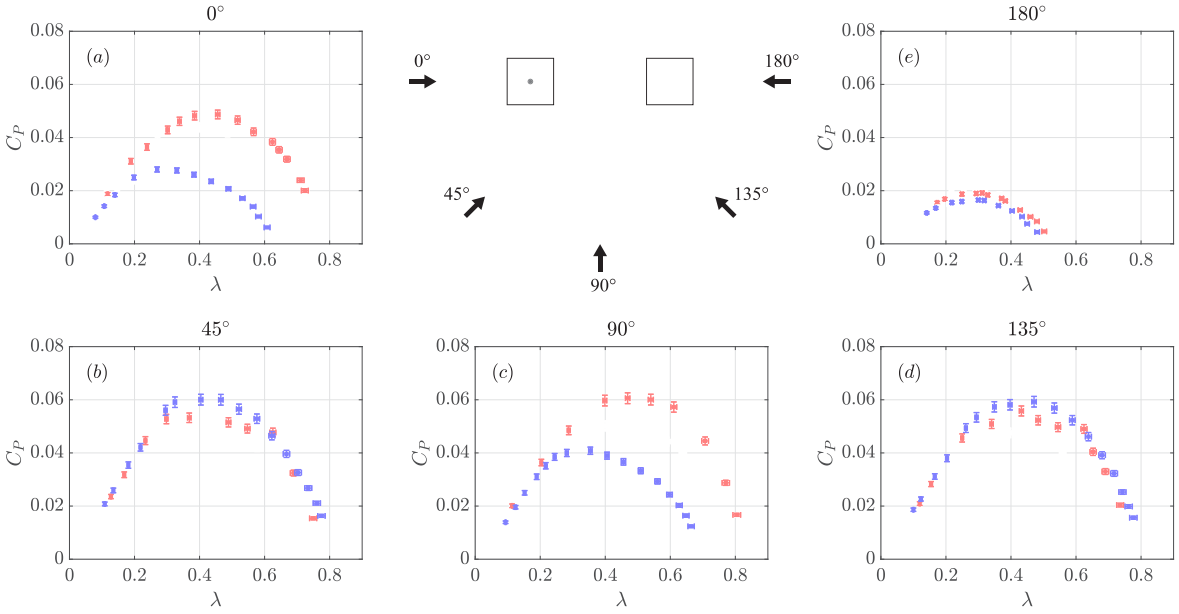

Fig. 10. Comparison of C_P-curves for the high and low turbine at position 2 for different wind directions. high turbine, low turbine.

integration limits within reasonable bounds did not alter the trends. Note that $\theta = 225°$, 270° and 315° were reconstructed from $\theta = 45°$, 90° and 135° by symmetry and included into the average for both methods to have correct weighting of all wind directions.

Both methods yield the same conclusions. Results are listed in Table 2, but for brevity only $\langle C_{P\,max} \rangle_\theta$ is discussed in the text. For the low turbine, this analysis suggests position 2 in the centre of the cube is the ideal position, followed by position 1 and position 3 which both have approximately 7% lower $\langle C_{P\,max} \rangle_\theta$. The ideal spot for the high turbine is also position 2, followed by position 3 and then position 1. The spread is slightly higher than for the low turbine with 12% difference between the best and worst position. Averaging both turbine heights for each position $\langle \langle C_{P\,max} \rangle_\theta \rangle$ consequently identifies position 2 as the ideal position for the examined turbine heights. Position 1 produces the lowest power output with position 3 in-between. The overall difference between the three positions is less than 10% when considering all wind directions and both turbine heights. Remarkably all three positions yield a higher $\langle \langle C_{P\,max} \rangle_\theta \rangle$ than $C_{P0,max}$.

The optimal wind direction θ_{opt} for every position and height, where the highest $C_{P\,max}$ was achieved, was also evaluated and listed in Table 2. For L1 and L2, the optimal wind direction is 45°. The diminished flow separation leads to higher streamwise velocity and thus better performance. For L3, the acceleration caused by the neighbouring cube at $\theta = 90°$ dominates, making this the ideal wind direction. For the high turbine, the recirculation bubble on top of the building is less problematic because accelerated fluid from above is entrained into the rotor area. This, in combination with the acceleration effect from the neighbouring building, makes $\theta = 90°$ the ideal wind direction for all three positions for the high turbine.

Generally, position 2 can be identified as the ideal spot from this analysis irrespective of turbine height (see Table 2). In an effort to allow for a more direct comparison of the two turbine heights, Fig. 10 compares the low and high turbine at position 2 for the examined wind directions. It is apparent that when the flow is orthogonal to the cube face, i.e., $\theta = 0°$ and 90°, the high turbine provides a significant benefit in performance compared to the low turbine. This is due to the flow separation at the upstream top edge of the cube for these cases, resulting in a large area of recirculating flow on top of the cube. For $\theta = 180°$, this effect is diminished due to the wake of the upstream cube dominating the flow field. Wind from $\theta = 45°$ and 135° results in a different flow pattern due to the lack of flow separation along the centre line of the cube. Thus, there is no benefit in a higher turbine for these directions. On the contrary, the low turbine actually gives a slightly higher power output for $\theta = 45°$ and 135°. This shows that even though the high turbine gives the higher overall power output, it remains important to consider the prevailing wind direction if such data is available.

5. Conclusions

The ideal position of a roof mounted Savonius (drag driven) vertical axis wind turbine was evaluated based on direct measurements of the converted power. The set-up consists of two neighbouring buildings modelled by surface mounted cubes. Three locations at two heights on one of the buildings were assessed for five representative wind directions. In addition, surface pressure measurements were used to obtain an understanding of flow patterns over the cubes. Assuming a uniform wind rose, thus taking into consideration all wind directions, the ideal position for a wind turbine is in the centre of a building for the examined turbine heights. However, for the individual wind directions the conclusions are nuanced. For wind from $\theta = 0°$ and $\theta = 180°$, the outside position farthest away from the other building is ideal for the low turbine. Contrarily wind from $\theta = 90°$ results in the inside position being the ideal location for the low turbine. The positional dependence of the converted power for $\theta = 45°$ and $\theta = 135°$ is lowest and the power output highest for the low turbine due to reduced flow separation on top of the building. The high turbine is generally less dependent on its position above a model building. The central location is within 10% of $C_{P\,max}$ for every wind direction and is the ideal spot for $\theta = 0°$, $\theta = 45°$ and $\theta = 135°$. The highest power output is recorded for $\theta = 90°$ at the inside position for the high turbine. Wind from $\theta = 180°$ yields the lowest C_P for both turbine heights with similar results. The high turbine performs significantly better than the low turbine for $\theta = 0°$ and $\theta = 90°$, whereas the low turbine has slight advantages for $\theta = 45°$ and $\theta = 135°$. The overall power output was found to exceed reference measurements in the unobstructed flow for every position and turbine height. In closing, a turbine placed in the centre of a building and as high as reasonably possible above the building, to remove it from the retarded flow region on the roof, is the most robust; however, if there is one dominate wind direction, a specific location, as suggested by the present results, may be superior.

CRediT authorship contribution statement

Yannick Jooss: Conceptualization, Methodology, Software, Validation, Formal analysis, Investigation, Writing – original draft, Visualization, Project administration. **Eivind Berg Rønning:** Methodology, Software, Validation, Formal analysis, Investigation, Writing – review & editing, Visualization. **R. Jason Hearst:** Conceptualization, Resources, Writing – review & editing, Supervision, Project administration, Funding acquisition. **Tania Bracchi:** Conceptualization, Resources, Writing – review & editing, Supervision, Project administration, Funding acquisition.

Declaration of competing interest

The authors declare that they have no known competing financial interests or personal relationships that could have appeared to influence the work reported in this paper.

Data availability

Data will be made available on request.

References

Abohela, I., Hamza, N., Dudek, S., 2013. Effect of roof shape, wind direction, building height and urban configuration on the energy yield and positioning of roof mounted wind turbines. Renew. Energy (ISSN: 0960-1481) 50, 1106–1118. http://dx.doi.org/10.1016/j.renene.2012.08.068.

Akwa, J.V., Vielmo, H.A., Petry, A.P., 2012. A review on the performance of Savonius wind turbines. Renew. Sustain. Energy Rev. (ISSN: 1364-0321) 16 (5), 3054–3064. http://dx.doi.org/10.1016/j.rser.2012.02.056.

Al-Quraan, A., Stathopoulos, T., Pillay, P., 2016. Comparison of wind tunnel and on site measurements for urban wind energy estimation of potential yield. J. Wind Eng. Ind. Aerodyn. (ISSN: 0167-6105) 158, 1–10. http://dx.doi.org/10.1016/j.jweia.2016.08.011.

Alexander, A.J., Holownia, B.P., 1978. Wind tunnel tests on a savonius rotor. J. Wind Eng. Ind. Aerodyn. (ISSN: 0167-6105) 3 (4), 343–351. http://dx.doi.org/10.1016/0167-6105(78)90037-5.

Aliferis, A.D., Jessen, M.S., Bracchi, T., Hearst, R.J., 2019. Performance and wake of a Savonius vertical-axis wind turbine under different incoming conditions. Wind Energy (ISSN: 1099-1824) 22 (9), 1260–1273. http://dx.doi.org/10.1002/we.2358.

Allard, M.A., Paraschivoiu, M., 2022. Power enhancement CFD based study of Darius wind turbine via roof corner placement. J. Renew. Sustain. Energy 14 (3), 033301. http://dx.doi.org/10.1063/5.0079971, Publisher: American Institute of Physics.

Bastankhah, M., Porté-Agel, F., 2017. A new miniature wind turbine for wind tunnel experiments. part I: designs and performance. Energies 10 (7), 908. http://dx.doi.org/10.3390/en10070908.

Castro, I.P., Robins, A.G., 1977. The flow around a surface-mounted cube in uniform and turbulent streams. J. Fluid Mech. 79 (2), 307–335. http://dx.doi.org/10.1017/S0022112077000172, (ISSN: 1469-7645, 0022-1120).

Chang, R.-D., Zuo, J., Zhao, Z.-Y., Zillante, G., Gan, X.-L., Soebarto, V., 2017. Evolving theories of sustainability and firms: History, future directions and implications for renewable energy research. Renew. Sustain. Energy Rev. (ISSN: 1364-0321) 72, 48–56. http://dx.doi.org/10.1016/j.rser.2017.01.029.

Cheng, Y., Lien, F.S., Yee, E., Sinclair, R., 2003. A comparison of large Eddy simulations with a standard k–ϵ Reynolds-averaged Navier–Stokes model for the prediction of a fully developed turbulent flow over a matrix of cubes. J. Wind Eng. Ind. Aerodyn. (ISSN: 0167-6105) 91 (11), 1301–1328. http://dx.doi.org/10.1016/j.jweia.2003.08.001.

Dabiri, J.O., 2011. Potential order-of-magnitude enhancement of wind farm power density via counter-rotating vertical-axis wind turbine arrays. J. Renew. Sustain. Energy 3 (4), 043104. http://dx.doi.org/10.1063/1.3608170, Publisher: American Institute of PhysicsAIP.

Danao, L.A., Eboibi, O., Howell, R., 2013. An experimental investigation into the influence of unsteady wind on the performance of a vertical axis wind turbine. Appl. Energy (ISSN: 0306-2619) 107, 403–411. http://dx.doi.org/10.1016/j.apenergy.2013.02.012.

Ferreira, M.A., Ganapathisubramani, B., 2021. Scale interactions in velocity and pressure within a turbulent boundary layer developing over a staggered-cube array. J. Fluid Mech. 910, http://dx.doi.org/10.1017/jfm.2020.999, (ISSN: 0022-1120, 1469-7645), Publisher: Cambridge University Press.

Gambuzza, S., Ganapathisubramani, B., 2021. The effects of free-stream turbulence on the performance of a model wind turbine. J. Renew. Sustain. Energy 13 (2), 023304. http://dx.doi.org/10.1063/5.0039168, Publisher: American Institute of Physics.

Gao, J., Agarwal, K., Katz, J., 2021. Experimental investigation of the three-dimensional flow structure around a pair of cubes immersed in the inner part of a turbulent channel flow. J. Fluid Mech. 918, http://dx.doi.org/10.1017/jfm.2021.184, (ISSN: 0022-1120, 1469-7645), Publisher: Cambridge University Press.

Ge, M., Gayme, D.F., Meneveau, C., 2021. Large-eddy simulation of wind turbines immersed in the wake of a cube-shaped building. Renew. Energy (ISSN: 0960-1481) 163, 1063–1077. http://dx.doi.org/10.1016/j.renene.2020.08.156.

Hearst, R.J., Gomit, G., Ganapathisubramani, B., 2016. Effect of turbulence on the wake of a wall-mounted cube. J. Fluid Mech. 804, 513–530. http://dx.doi.org/10.1017/jfm.2016.565, (ISSN: 0022-1120, 1469-7645).

Hui, I., Cain, B.E., Dabiri, J.O., 2018. Public receptiveness of vertical axis wind turbines. Energy Policy (ISSN: 0301-4215) 112, 258–271. http://dx.doi.org/10.1016/j.enpol.2017.10.028.

Jooss, Y., Bolis, R., Bracchi, T., Hearst, R.J., 2022. Flow field and performance of a vertical-axis wind turbine on model buildings. Flow (ISSN: 2633-4259) 2, http://dx.doi.org/10.1017/flo.2022.3, Publisher: Cambridge University Press.

Kc, A., Whale, J., Urmee, T., 2019. Urban wind conditions and small wind turbines in the built environment: A review. Renew. Energy (ISSN: 0960-1481) 131, 268–283. http://dx.doi.org/10.1016/j.renene.2018.07.050.

Kooiman, S., Tullis, S., 2010. Response of a vertical axis wind turbine to time varying wind conditions found within the urban environment. Wind Eng. (ISSN: 0309-524X) 34 (4), 389–401. http://dx.doi.org/10.1260/0309-524X.34.4.389, Publisher: SAGE Publications.

Kozmar, H., 2020. Surface pressure on a cubic building exerted by conical vortices. J. Fluids Struct. (ISSN: 0889-9746) 92, 102801. http://dx.doi.org/10.1016/j.jfluidstructs.2019.102801.

Kozmar, H., 2021. Flow, turbulence and surface pressure on a wall-mounted cube in turbulent boundary layers. J. Wind Eng. Ind. Aerodyn. (ISSN: 0167-6105) 210, 104503. http://dx.doi.org/10.1016/j.jweia.2020.104503.

Kumbernuss, J., Chen, J., Yang, H.X., Lu, L., 2012. Investigation into the relationship of the overlap ratio and shift angle of double stage three bladed vertical axis wind turbine (VAWT). J. Wind Eng. Ind. Aerodyn. (ISSN: 0167-6105) 107–108, 57–75. http://dx.doi.org/10.1016/j.jweia.2012.03.021.

Larin, P., Paraschivoiu, M., Aygun, C., 2016. CFD based synergistic analysis of wind turbines for roof mounted integration. J. Wind Eng. Ind. Aerodyn. (ISSN: 0167-6105) 156, 1–13. http://dx.doi.org/10.1016/j.jweia.2016.06.007.

Ledo, L., Kosasih, P.B., Cooper, P., 2011. Roof mounting site analysis for micro-wind turbines. Renew. Energy (ISSN: 0960-1481) 36 (5), 1379–1391. http://dx.doi.org/10.1016/j.renene.2010.10.030.

Li, D., Wang, S., Yuan, P., 2010. A review of micro wind turbines in the built environment. In: 2010 Asia-Pacific Power and Energy Engineering Conference. pp. 1–4. http://dx.doi.org/10.1109/APPEEC.2010.5448223, ISSN: 2157-4847.

Loganathan, B., Mustary, I., Chowdhury, H., Alam, F., 2017. Effect of turbulence on a savonius type micro wind turbine. Energy Procedia (ISSN: 1876-6102) 110, 549–554. http://dx.doi.org/10.1016/j.egypro.2017.03.183.

Martinuzzi, R.J., Havel, B., 2004. Vortex shedding from two surface-mounted cubes in tandem. Int. J. Heat Fluid Flow (ISSN: 0142-727X) 25 (3), 364–372. http://dx.doi.org/10.1016/j.ijheatfluidflow.2004.02.003.

Medici, D., Ivanell, S., Dahlberg, J.-A., Alfredsson, P.H., 2011. The upstream flow of a wind turbine: blockage effect. Wind Energy (ISSN: 1099-1824) 14 (5), 691–697. http://dx.doi.org/10.1002/we.451.

Meinders, E.R., Hanjalić, K., 1999. Vortex structure and heat transfer in turbulent flow over a wall-mounted matrix of cubes. Int. J. Heat Fluid Flow (ISSN: 0142-727X) 20 (3), 255–267. http://dx.doi.org/10.1016/S0142-727X(99)00016-8.

Mertens, S., 2003. The energy yield of roof mounted wind turbines. Wind Eng. (ISSN: 0309-524X) 27 (6), 507–518. http://dx.doi.org/10.1260/030952403773617472, Publisher: SAGE Publications.

Mertens, S., 2006. Wind energy in the built environment concentrator effects of buildings.

Millward-Hopkins, J.T., Tomlin, A.S., Ma, L., Ingham, D., Pourkashanian, M., 2012. The predictability of above roof wind resource in the urban roughness sublayer. Wind Energy (ISSN: 1099-1824) 15 (2), 225–243. http://dx.doi.org/10.1002/we.463.

Natarajan, V., Chyu, M.K., 1994. Effect of flow angle-of-attack on the local heat/mass transfer from a wall-mounted cube. J. Heat Transfer (ISSN: 0022-1481) 116 (3), 552–560. http://dx.doi.org/10.1115/1.2910906.

Oke, T.R., 1976. The distinction between canopy and boundary-layer urban heat islands. Atmosphere (ISSN: 0004-6973) 14 (4), 268–277. http://dx.doi.org/10.1080/00046973.1976.9648422.

Porté-Agel, F., Bastankhah, M., Shamsoddin, S., 2020. Wind-turbine and wind-farm flows: a review. Bound.-Lay. Meteorol. (ISSN: 1573-1472) 174 (1), 1–59. http://dx.doi.org/10.1007/s10546-019-00473-0.

Raupach, M.R., Antonia, R.A., Rajagopalan, S., 1991. Rough-wall turbulent boundary layers. Appl. Mech. Rev. (ISSN: 0003-6900) 44 (1), 1–25. http://dx.doi.org/10.1115/1.3119492.

Rezaeiha, A., Montazeri, H., Blocken, B., 2020. A framework for preliminary large-scale urban wind energy potential assessment: Roof-mounted wind turbines. Energy Convers. Manage. (ISSN: 0196-8904) 214, 112770. http://dx.doi.org/10.1016/j.enconman.2020.112770.

Šarkić Glumac, A., Hemida, H., Höffer, R., 2018. Wind energy potential above a high-rise building influenced by neighboring buildings: An experimental investigation. J. Wind Eng. Ind. Aerodyn. (ISSN: 0167-6105) 175, 32–42. http://dx.doi.org/10.1016/j.jweia.2018.01.022.

Scheurich, F., Brown, R.E., 2013. Modelling the aerodynamics of vertical-axis wind turbines in unsteady wind conditions. Wind Energy (ISSN: 1099-1824) 16 (1), 91–107. http://dx.doi.org/10.1002/we.532, _eprint: https://onlinelibrary.wiley.com/doi/pdf/10.1002/we.532.

Shahizare, B., Nik-Ghazali, N., Chong, W.T., Tabatabaeikia, S., Izadyar, N., Esmaeilzadeh, A., 2016. Novel investigation of the different Omni-direction-guide-vane angles effects on the urban vertical axis wind turbine output power via three-dimensional numerical simulation. Energy Convers. Manage. (ISSN: 0196-8904) 117, 206–217. http://dx.doi.org/10.1016/j.enconman.2016.03.034.

Shamsoddin, S., Porté-Agel, F., 2014. Large eddy simulation of vertical axis wind turbine wakes. Energies 7 (2), 890–912. http://dx.doi.org/10.3390/en7020890, Number: 2 Publisher: Multidisciplinary Digital Publishing Institute.

Škvorc, P., Kozmar, H., 2021. Wind energy harnessing on tall buildings in urban environments. Renew. Sustain. Energy Rev. (ISSN: 1364-0321) 152, 111662. http://dx.doi.org/10.1016/j.rser.2021.111662.

Stathopoulos, T., Alrawashdeh, H., Al-Quraan, A., Blocken, B., Dilimulati, A., Paraschivoiu, M., Pilay, P., 2018. Urban wind energy: Some views on potential and challenges. J. Wind Eng. Ind. Aerodyn. (ISSN: 0167-6105) 179, 146–157. http://dx.doi.org/10.1016/j.jweia.2018.05.018.

Toja-Silva, F., Peralta, C., Lopez-Garcia, O., Navarro, J., Cruz, I., 2015. On roof geometry for urban wind energy exploitation in high-rise buildings. Computation 3 (2), 299–325.

UNFCCC, 2015. The paris agreement.

Vita, G., Šarkić Glumac, A., Hemida, H., Salvadori, S., Baniotopoulos, C., 2020. On the wind energy resource above high-rise buildings. Energies 13 (14), 3641. http://dx.doi.org/10.3390/en13143641, Number: 14 Publisher: Multidisciplinary Digital Publishing Institute.

Walker, S.L., 2011. Building mounted wind turbines and their suitability for the urban scale—A review of methods of estimating urban wind resource. Energy Build. (ISSN: 0378-7788) 43 (8), 1852–1862. http://dx.doi.org/10.1016/j.enbuild.2011.03.032.

Wang, L., Li, D., Gao, Z., Sun, T., Guo, X., Bou-Zeid, E., 2014. Turbulent transport of momentum and scalars above an urban canopy. Bound.-Lay. Meteorol. (ISSN: 1573-1472) 150 (3), 485–511. http://dx.doi.org/10.1007/s10546-013-9877-z.

Wekesa, D.W., Wang, C., Wei, Y., Zhu, W., 2016. Experimental and numerical study of turbulence effect on aerodynamic performance of a small-scale vertical axis wind turbine. J. Wind Eng. Ind. Aerodyn. (ISSN: 0167-6105) 157, 1–14. http://dx.doi.org/10.1016/j.jweia.2016.07.018.

Wheeler, A.J., Ganji, A.R., 1996. Introduction to Engineering Experimentation, Vol. 199, No. 6. Prentice Hall New Jersey.

Xie, Z., Castro, I.P., 2006. LES and RANS for turbulent flow over arrays of wall-mounted obstacles. Flow Turbul. Combust. (ISSN: 1573-1987) 76 (3), 291. http://dx.doi.org/10.1007/s10494-006-9018-6.

Xie, Z.-T., Coceal, O., Castro, I.P., 2008. Large-eddy simulation of flows over random urban-like obstacles. Bound.-Lay. Meteorol. (ISSN: 1573-1472) 129 (1), 1. http://dx.doi.org/10.1007/s10546-008-9290-1.

Yakhot, A., Liu, H., Nikitin, N., 2006. Turbulent flow around a wall-mounted cube: A direct numerical simulation. Int. J. Heat Fluid Flow (ISSN: 0142-727X) 27 (6), 994–1009. http://dx.doi.org/10.1016/j.ijheatfluidflow.2006.02.026.

Yan, S., Shi, S., Chen, X., Wang, X., Mao, L., Liu, X., 2018. Numerical simulations of flow interactions between steep hill terrain and large scale wind turbine. Energy (ISSN: 0360-5442) 151, 740–747. http://dx.doi.org/10.1016/j.energy.2017.12.075.

Zhang, S., Du, B., Ge, M., Zuo, Y., 2022. Study on the operation of small rooftop wind turbines and its effect on the wind environment in blocks. Renew. Energy (ISSN: 0960-1481) 183, 708–718. http://dx.doi.org/10.1016/j.renene.2021.11.059.

Zhou, H., Lu, Y., Liu, X., Chang, R., Wang, B., 2017. Harvesting wind energy in low-rise residential buildings: Design and optimization of building forms. J. Cleaner Prod. (ISSN: 0959-6526) 167, 306–316. http://dx.doi.org/10.1016/j.jclepro.2017.08.166.